Physics Letters B 285 (1992) 10–14
North-Holland

PHYSICS LETTERS B

Multifragment emission in $^{36}Ar+^{197}Au$ and $^{129}Xe+^{197}Au$ collisions. Percolation model

L. Phair, W. Bauer, D.R. Bowman, N. Carlin [1], R.T. de Souza [2], C.K. Gelbke, W.G. Gong [3], Y.D. Kim [2], M.A. Lisa, W.G. Lynch, G.F. Peaslee, M.B. Tsang, C. Williams, F. Zhu

National Superconducting Cyclotron Laboratory and Department of Physics and Astronomy, Michigan State University, East Lansing, MI 48824, USA

N. Colonna, K. Hanold, M.A. McMahan, G.J. Wozniak and L.G. Moretto

Nuclear Science Division and Accelerator and Fusion Research Division, Lawrence Berkeley Laboratory, Berkeley, CA 94720, USA

Received 10 January 1992

Relative abundances of intermediate mass fragments and light particles measured for $^{36}Ar+^{197}Au$ collisions at $E/A=50$, 80 and 110 MeV lie within the range of percolation model predictions, but for $^{129}Xe+^{197}Au$ collisions at $E/A=50$ MeV, the percolation model predicts too small admixtures of intermediate mass fragments among the emitted charged particles.

Multifragment disintegrations of highly excited nuclear systems might carry information about the equation of state and the liquid–gas phase transition of low density nuclear matter (see refs. [1–5] and references given therein). A number of theoretical investigations of phase transitions in finite nuclear systems have been based on percolation models [6–10]. Percolation models are attractive, since they exhibit a well-defined phase transition for infinite systems and since they allow straightforward generalizations to finite systems. They have been rather successful [6] in describing the observed [2] power-law behavior of measured fragment mass distributions and in developing techniques to extract critical exponents. During the last year, a number of new experimental results on multifragment reactions have been reported [11–17] which allow more detailed comparisons with model calculations. In this letter we compare predictions of the bond-percolation model [6] to fragment yields measured [16,17] with a low-threshold 4π detector for the reactions $^{129}Xe+^{197}Au$ at $E/A=50$ MeV and $^{36}Ar+^{197}Au$ at $E/A=50$, 80, 110 MeV.

The experiments were performed with beams from the K1200 cyclotron of the NSCL at Michigan State University. Reaction products were detected with the MSU Miniball phoswich detector array [18] which consists of 11 azimuthally symmetric rings subtending polar angles of $\Theta_{lab}=9°-160°$. Each phoswich detector consisted of a 40 μm thick plastic scintillator foil backed by a 2 cm thick CsI(Tl) crystal. (For detectors in Ring 1, the scintillator foil was 50 μm thick.) For the $^{129}Xe+^{197}Au$ reaction, the most forward angles were covered by a 16-element hodoscope, each element of which consisted of two position-sensitive solid-state detectors (300 μm and 5 mm thick) and a 7.6 cm thick plastic scintillator [19]. Fragments detected in the Miniball were identified by element for $Z\approx 1$–20; representative detection thresholds were 2, 3, and 4 MeV/nucleon for $Z=3$, 10, and 18 fragments, respectively. Fragments detected in the forward array were identified by element for $Z=1$–54; representative detection thresholds were 6, 13, 21, and 27 MeV/nucleon for $Z=2$,

[1] Present address: Instituto de Física, Universidade de São Paulo, C.P. 20516, CEP 01498, São Paulo, Brazil.

[2] Present address: IUCF and Department of Chemistry, Indiana University, Bloomington, IN 47405, USA.

[3] Present address: Nuclear Science Division, Lawrence Berkeley Laboratory, Berkeley, CA 94720, USA.

8, 20, and 54 fragments, respectively. Additional technical details can be found in refs. [16–19].

For a given event, we define the charged particle multiplicity N_C as the number of detectors in which at least one charged particle is recorded, including low energy fragments stopped in the plastic scintillator foils. Slightly different from previous analyses, the multiplicity of intermediate mass fragments (IMF, $Z=3$–20) excludes low energy heavy fragments stopped in the scintillator foils. As a result, the IMF multiplicities are slightly lower than reported in refs. [16,17].

Calculations were performed with the bond percolation model of ref. [6]. In this model, the nucleus is considered to be a cubic lattice, the sites of which are randomly occupied by protons and neutrons. Initially, all nucleons are connected in one cluster. The bonds between the sites are randomly broken with a probability p. Each nucleon is assigned a random momentum consistent with the momentum distribution of a Fermi gas of temperature T calculated [6] from the bond-breaking probability as $T=11.7\sqrt{p}$ MeV. Emitted fragments are defined in terms of connected clusters. Initial fragment energies are calculated from the total momenta of the clusters. Final kinetic energies are calculated by incorporating the final state Coulomb repulsion between the fragments. For this purpose a given fragment partition is translated into a spatial distribution of clusters characterized by an average freeze-out density $\rho=0.2\rho_0$, where $\rho_0=0.17$ fm^{-3} is the density of normal nuclear matter. (Different choices of the freeze-out density lead to slightly different shapes of the low energy portion of the energy spectrum due to changes in the Coulomb repulsion between the fragments. Such changes are of minor importance for the present investigation.) As a final step, all energies are transformed via galilean transformations from the center-of-mass system into the laboratory rest frame. To allow meaningful comparisons with our data, we present calculations filtered by the response of the experimental apparatus. To illustrate the magnitude of instrumental distortions we also show unfiltered calculations.

Fig. 1 provides approximate scales between the "reduced" impact parameter $\hat{b}$ and the charged particle multiplicity N_C, obtained from the simple geometric prescription [20]

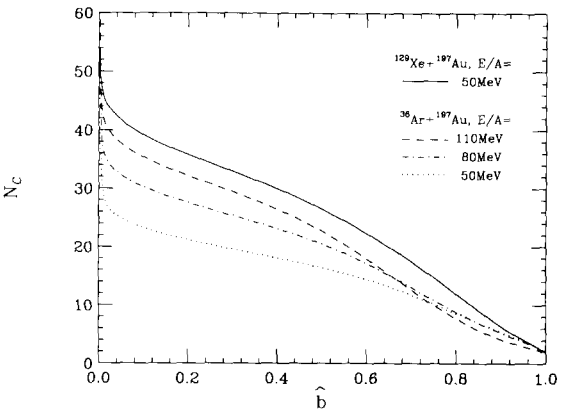

Fig. 1. Relation between charged particle multiplicity N_C and reduced impact parameter, $\hat{b}=b/b_{max}$, as determined from eq. (1).

$$\hat{b}(N_C)=\frac{1}{\sqrt{\sigma_R}}\left(\sum_{N'_C=N_C}^{\infty}\sigma(N'_C)\right)^{1/2}, \qquad (1)$$

where $\sigma(N'_C)$ is the cross section for events with detected charged particle multiplicity N'_C and σ_R is the reaction cross section for $N_C\geq 2$.

Elemental multiplicity distributions measured for central ($\hat{b}\leq 0.3$) $^{36}Ar+^{197}Au$ and $^{129}Xe+^{197}Au$ collisions are shown (as points) in the top and bottom panels of fig. 2. These distributions were obtained by integrating all identified fragments over all detectors. The cuts on N_C are indicated in the figure. All elemental distributions exhibit qualitatively similar shapes. For the $^{36}Ar+^{197}Au$ system, they become slightly steeper with increasing bombarding energy. Multiplicities of heavier IMFs are larger for the $^{129}Xe+^{197}Au$ system than for the $^{36}Ar+^{197}Au$ system. Due to incomplete geometrical coverage and finite detection thresholds, only a fraction of the total charge is detected. The N_C-dependence of the detected charge has been presented in refs. [17,18]. In central collisions, the average detected charge is slightly less than 40% of the total charge for $^{36}Ar+^{197}Au$ at $E/A=50$ MeV, and of the order of 60% for $^{36}Ar+^{197}Au$ at $E/A=110$ MeV and $^{129}Xe+^{197}Au$ at $E/A=50$ MeV [17,18]

The curves in fig. 2 depict elemental multiplicities predicted by the bond percolation model of ref. [6]. The dashed, solid, and dotted curves show the results of filtered calculations for bond-breaking probabilities $p=0.6$, 0.7, and 0.8, respectively; the dot-dashed

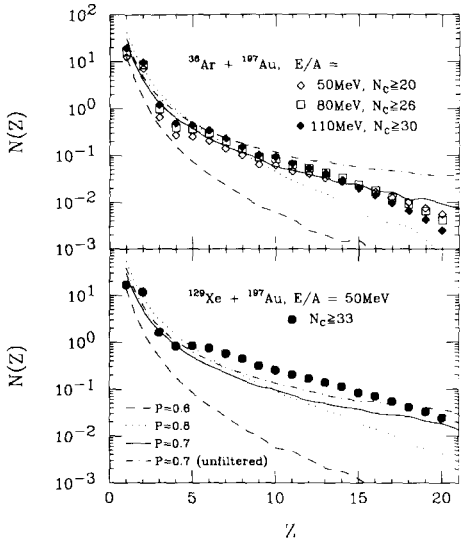

Fig. 2. Elemental multiplicity distributions detected in ^{36}Ar+^{197}Au and ^{129}Xe+^{197}Au collisions at the indicated energies. The curves represent results from percolation calculations for the indicated bond-breaking probabilities p. Details are given in the text.

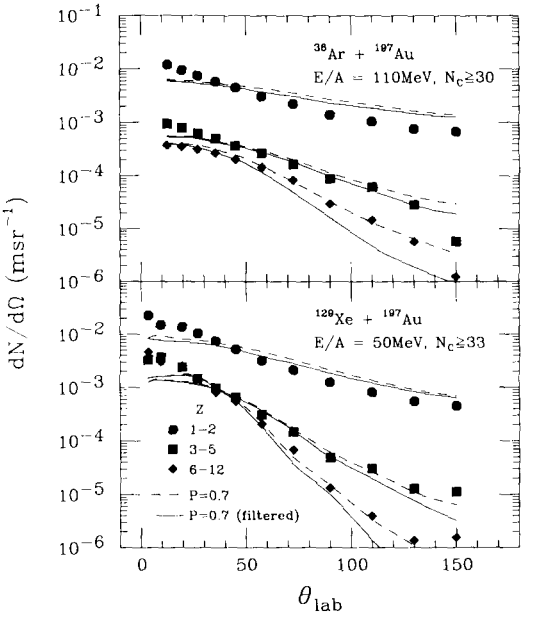

Fig. 3. Angular multiplicity distributions of light particles ($Z=1$, 2: circles), and intermediate mass fragments of $Z=3$–5 (squares) and $Z=6$–12 (diamonds) detected in ^{36}Ar+^{197}Au and ^{129}Xe+^{197}Au collisions at the indicated energies. Solid and dashed curves show filtered and unfiltered percolation calculations, respectively. Details are given in the text.

curves represent unfiltered calculations for $p=0.7$. In the percolation model, the critical point at $p=0.7$ marks a second order phase transition: for $p<0.7$, a heavy percolation cluster (or fusion-residue) exists, but for $p>0.7$, the system breaks up completely. Calculations performed for bond-breaking probabilities much larger or smaller than the critical value predict Z-distributions which are too steep. For the ^{36}Ar+^{197}Au reactions, the overall magnitudes and shapes of the experimental Z-distributions are in reasonable agreement with predictions of the percolation model when the bond-breaking parameter is taken close to the critical value. However, for the ^{129}Xe+^{197}Au reaction, the percolation model underpredicts the yield of heavier fragments ($Z \approx 6$–20) for any choice of the bond-breaking parameter.

Representative angular distributions of emitted particles are shown in fig. 3. The top and bottom panels show results for the ^{36}Ar+^{197}Au reaction at $E/A=110$ MeV and for the ^{129}Xe+^{197}Au reaction at $E/A=50$ MeV, respectively. The angular distributions are shown for three different ranges of element numbers, $Z=1$–2 (circles), $Z=3$–5 (squares), and $Z=6$–12 (diamonds). For both systems, the angular distributions become more forward peaked with increasing fragment charge. Angular distributions for the ^{129}Xe+^{197}Au system are more forward peaked than those for the ^{36}Ar+^{197}Au system. These effects are largely due to kinematics. Differences between the angular distributions of the two reactions arise primarily from the larger velocity of the emitting source of the ^{129}Xe+^{197}Au system.

The solid and dashed curves in fig. 3 show filtered and unfiltered results of percolation calculations, respectively. To facilitate a better comparison of shapes between observed and predicted angular distributions, the calculated and filtered angular distributions were normalized to the experimental yields at $\theta=45°$. The shapes of the experimental angular distributions are reasonably well reproduced by the calculations. Some discrepancies between theoretical and experimental angular distributions exist for lighter fragments for which preequilibrium contributions lead to somewhat more forward peaked angular distributions than predicted by our calculations. Similar discrepancies exist for other treatments in which statistical equilibrium is assumed.

Microscopic transport calculations [21] capable of treating nonequilibrium fragment emission predict fewer fragments [17,18] than observed experimentally. Dynamics, as treated by these models, may not play the decisive role in fragment production. In this context, it is interesting to neglect dynamical effects and explore whether fragment formation could be dominated by the geometric considerations contained in the percolation ansatz. For this purpose, the calculated angular distributions may be sufficiently realistic to assess the effects of instrumental distortions on the energy- and angle-integrated particle distributions presented in figs. 2 and 4.

As was already evident from fig. 2, the percolation model can reproduce the relative IMF abundance observed in central $^{36}Ar+^{197}Au$ collisions, but predicts too small IMF admixtures for central $^{129}Xe+^{197}Au$ collisions. This failure is depicted more clearly in fig. 4. Points in the figure [16,17] show the average IMF multiplicity $\langle N_{IMF} \rangle$ as a function of charged particle multiplicity N_C; thick and thin curves represent results of filtered and unfiltered percolation calculations, respectively, using the critical bond-breaking parameter, $p=0.7$. For the percolation model, these calculations give upper bounds for the admixture of IMFs among the emitted charged particles. Smaller IMF admixtures can be obtained by using larger or smaller bond-breaking parameters.

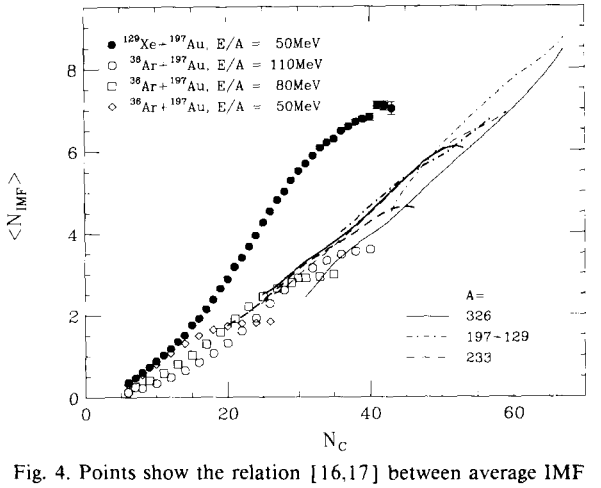

Fig. 4. Points show the relation [16,17] between average IMF and charged particle multiplicities for $^{36}Ar+^{197}Au$ and $^{129}Xe+^{197}Au$ collisions at the indicated energies. Thick and thin curves show the results of filtered and unfiltered percolation calculations, respectively. Details are given in the text.

The dashed curves in fig. 4 show percolation calculations for the combined $^{36}Ar+^{197}Au$ system. For this system, filtered and unfiltered IMF admixtures are very similar, and the relative abundance of IMFs observed in central collisions can be reproduced by the model calculations.

The solid curves in fig. 4 represent percolation calculations for the combined $^{129}Xe+^{197}Au$ system. Here, the filtered calculations represent slightly higher IMF admixtures than the unfiltered calculations. This effect is largely due to an increased IMF detection efficiency resulting from the larger center-of-mass velocity of the Xe+Au center-of-mass system. However, both filtered and unfiltered calculations predict too small IMF admixtures. This failure is most dramatic for central $^{129}Xe+^{197}Au$ collisions for which the comparison is most meaningful.

As an alternative scenario, we have also performed percolation model calculations for the separate multifragment decay of projectile and target nuclei. The unfiltered calculations, shown by the thin dot-dashed curve, predict slightly higher IMF admixtures. The thick dot-dashed curve illustrates the effect of filtering for an extreme two-source scenario in which the relative velocity of projectile and target was reduced by only 50% from the initial value, taking total momentum conservation into account. Even in such an extreme scenario, the major discrepancy remains.

High resolution coincidence experiments indicate that a significant portion of primary fragments should be produced in highly excited, particle unbound states which decay by light particle emission [22]. Such sequential decay processes will result in secondary fragment yields which are smaller and secondary light particle yields which are larger than the corresponding primary yields. The portion of primary fragments may therefore be even larger than the portion of detected particle-stable secondary fragments. This aggravates the failure of the percolation model of predicting a sufficiently large admixture of IMFs among the particles emitted in the $^{129}Xe+^{197}Au$ reaction.

The inability of the bond-percolation model to reproduce the large fraction of intermediate mass fragments among the charged particles emitted in the $^{129}Xe+^{197}Au$ reaction is unexpected and represents, to our knowledge, its first significant failure. The model is only one representation of a large number of phase transition models, which all belong to the

same universality class and may therefore show similar deficiencies. Our results raise a number of questions: Should one rule out related phase transition models, or is this failure unique to purely geometric approaches reflected by the percolation ansatz? Are dynamical effects during the early nonequilibrium stages of the reaction responsible for such enhanced fragment yields or does it suffice to incorporate the dynamics of collective expansion or rotation, both of which occur on slightly slower time scales? These questions cannot yet be answered with certainty.

This work is based upon work supported by the National Science Foundation under Grant numbers PHY-86-11210, PHY-89-13815, PH9017077 and the US Department of Energy under Contract No. DE-AC03-76SF00098. W.G. Lynch acknowledges the receipt a of US Presidential Young Investigator Award and N. Carlin acknowledges partial support by the FAPESP, Brazil.

References

[1] G. Bertsch and P.J. Siemens, Phys. Lett. B 126 (1983) 9.
[2] A.S. Hirsch et al., Phys. Rev. C 29 (1984) 508.
[3] L.P. Cernai and J. Kapusta, Phys. Rep. 131 (1986) 223.
[4] W.G. Lynch, Annu. Rev. Nucl. Sci. 37 (1987) 493.
[5] D.H.E. Gross, Rep. Prog. Phys. 53 (1990) 605.
[6] W. Bauer et al., Phys. Lett. B 150 (1985) 53; Nucl. Phys. A 452 (1986) 699; Phys. Rev. C 38 (1988) 1927.
[7] X. Campi, J. Phys. A 19 (1986) L917; Phys. Lett. B 208 (1988) 351.
[8] H. Ngô et al., Z. Phys. A 337 (1990) 81.
[9] T.S. Biro et al., Nucl. Phys. A 459 (1986) 692.
[10] H.R. Jaqaman et al., Nucl. Phys. A 514 (1990) 327.
[11] E. Piasecki et al., Phys. Rev. Lett. 66 (1991) 1291.
[12] Y. Blumenfeld et al., Phys. Rev. Lett. 66 (1991) 576.
[13] D.R. Bowman et al., Nucl. Phys. A 523 (1991) 386.
[14] S.J. Yennello et al., Phys. Rev. Lett. 67 (1991) 671.
[15] C.A. Ogilvie et al., Phys. Rev. Lett. 67 (1991) 1214.
[16] R.T. de Souza et al., Phys. Lett. B 268 (1991) 6.
[17] D.R. Bowman et al., Phys. Rev. Lett. 67 (1991) 1527.
[18] R.T. de Souza et al., Nucl. Instrum. Methods A 295 (1990) 109.
[19] W.L. Kehoe et al., Lawrence Berkeley Laboratory preprint # LBL-31005.
[20] C. Cavata et al., Phys. Rev. C 42 (1990) 1760.
[21] D.H. Boal and J.N. Glosli, Phys. Rev. C 37 (1988) 91; C 42 (1990) R502.
[22] T.K. Nayak et al., Phys. Rev. C 45 (1992) 132, and references therein.